

# Direct Pose Estimation with a Monocular Camera

Darius Burschka and Elmar Mair

Department of Informatics  
Technische Universität München, Germany  
{burschka|elmar.mair}@mytum.de

**Abstract.** We present a direct method to calculate a 6DoF pose change of a monocular camera for mobile navigation. The calculated pose is estimated up to a constant unknown scale parameter that is kept constant over the entire reconstruction process. This method allows a direct calculation of the metric position and rotation without any necessity to fuse the information in a probabilistic approach over longer frame sequence as it is the case in most currently used VSLAM approaches. The algorithm provides two novel aspects to the field of monocular navigation. It allows a direct pose estimation without any a-priori knowledge about the world directly from any two images and it provides a quality measure for the estimated motion parameters that allows to fuse the resulting information in Kalman Filters.

We present the mathematical formulation of the approach together with experimental validation on real scene images.

## 1 Motivation

Localization is an essential task in most applications of a mobile or a manipulation system. It can be subdivided into two categories of the initial (global) localization and the relative localization. While the former requires an identification of known reference structures in the camera image to find the current pose relative to a known, a-priori map [9], often it is merely necessary to register correctly the relative position changes in consecutive image frames.

Many localization approaches for indoor applications use simplifications like assumptions about planarity of the imaged objects in the scene or assume a restricted motion in the ground plane of the floor that allows to derive the metric navigation parameters from differences in the images using Image Jacobians in vision-based control approaches. A true 6DoF localization requires a significant computational effort to calculate the parameters while solving an octal polynomial equation [8] or estimating the pose with a Bayesian minimization approach utilizing intersections of uncertainty ellipsoids to find the true position of the imaged points from a longer sequence of images [3]. While the first solution still requires a sampling to find the true solution of the equation due to the high complexity of the problem, the second one can calculate the result only after a

motion sequence with strongly varying direction of motion of the camera that helps to reduce the uncertainty about the position of the physical point.

A common used solutions to this problem are structure from motion approaches like the *eight point algorithm* [7] and its derivatives using as few as five corresponding points between the two images. Another approach is to use homographies to estimate the motion parameters in case that the corresponding points all are on a planar surface. These approaches provide a solution to the motion parameters (R,T - rotation matrix, translation vector) but are very sensitive to the ill conditioned point configurations and to outliers. Usually, the noise in the point detection does not allow to detect ill-conditioned cases and the system needs to cope with wrong estimate without any additional information about the covariance of the estimated values. Our method follows the idea of metric reconstruction from the absolute conic  $\Omega_\infty$  [11] for the calculation of the pose parameters for any point configuration providing correct covariance values for all estimates. Our contribution is a robust implementation of the algorithm suppressing outliers in the matches between the two images using RANSAC and a correct calculation of covariance values for the resulting pose estimation.

Since the projection in a monocular camera results in a loss of one dimension, the estimation of the three-dimensional parameters in space usually requires a metric reference to the surrounding world, a 3D model, that is used to scale the result of the image processing back to Cartesian coordinates. Assuming that the projective geometry of the camera is modeled by perspective projection [6], a point,  ${}^cP = (x, y, z)^T$ , whose coordinates are expressed with respect to the camera coordinate frame  $c$ , will project onto the image plane with coordinates  $p = (u, \nu)^T$ , given by

$$\pi({}^cP) = \begin{pmatrix} u \\ \nu \end{pmatrix} = \frac{f}{z} \begin{pmatrix} x \\ y \end{pmatrix} \quad (1)$$

Points in the image correspond to an internal model of the environment that is stored in 3D coordinates  ${}^mP$ .

Localization with a monocular camera system is in this case formulated as estimation of the transformation matrix  ${}^c x_m$  such that an image point  $p = (u, \nu)^T$  corresponds to an actual observation in the camera image for any visible model point  ${}^mP$ .

$$p = \pi({}^c x_m({}^mP)) \quad (2)$$

In many cases the initial position of the system is known or not relevant, since the initial frame may define the starting position. We propose a navigation system that operates in the image space of the camera for this domain of applications. The system maintains the correspondences between the “model” and the world based on a simple landmark tracking since both the model and the perception are defined in the same coordinate frame of the camera projection  $p = (u, \nu)^T$ .

The paper is structured as follows, in the following section we present the algorithms used for the estimation of the 3D rotation matrix from the points on

the "horizon" and the way how the tracked points are classified if far away from the camera. We describe the way the system processes the image data to estimate the translational component in all three degrees of freedom. This estimation is possible only up to a scale. In Section 3 we evaluate the accuracy of the system for different motion parameters. We conclude with an evaluation of the system performance and our future plans.

## 2 Imaging Properties of a Monocular Camera

As mentioned already above, a projection in a camera image results in a reduction of the dimensionality of the scene. The information about the radial distance to the point  $\lambda_i$  is lost in the projection (Fig. 1).

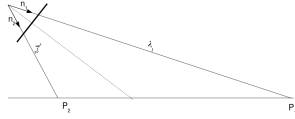


**Fig. 1.** Radial distance  $\lambda_i$  is lost during the camera projection. Only the direction  $\mathbf{n}_i$  to the imaged point can be obtained from the camera image.

Only the direction vector  $\vec{n}_i^\lambda$  can be calculated from the camera projection to:

$$\vec{k}_i = \begin{pmatrix} \frac{(u_{pi}-C_x) \cdot s_x}{f} \\ \frac{(v_{pi}-C_y) \cdot s_y}{f} \\ 1 \end{pmatrix} \Rightarrow \vec{n}_i^\lambda = \frac{1}{\|\vec{k}_i^\lambda\|} \vec{k}_i \quad (3)$$

with  $(u_{pi}, v_{pi})$  being the pixel coordinates of a point.  $(C_x, C_y)$  represent the position of the optical center in the camera image,  $(s_x, s_y)$  are the pixel sizes on the camera chip, and  $f$  is the focal length of the camera. This transformation removes all dependencies from the calibration parameters, like the parameters of the actual optical lens and its mount relative to the camera image. It transforms the image information into a pure geometric line of sight representation.

An arbitrary motion of the camera in space can be defined by the 3 translation parameters  $\vec{T} = (XYZ)^T$  and a rotation matrix  $R$ . The motion can be observed as an apparent motion of a point from a position  $\vec{P}$  to a position  $\vec{P}'$

$$\vec{P}' = R^T \vec{P} - \vec{T} \quad (4)$$

Optical flow approaches have already proven that these two motions result in specific shifts in the projected camera image. The resulting transformation on the imaged points corresponds to a sum of the motions induced by the rotation of the system  $R$  and the consecutive translation  $\vec{T}$ . Since we can write any point

in the world according to Fig. 1 as a product of its direction of view  $n_i$  and the radial distance  $\lambda_i$ , we can write (4) in the following form

$$\lambda_i \vec{n}_i = \lambda_i R^T \vec{n}_i^\lambda - \vec{T} \quad (5)$$

If we were able to neglect one of the influences on the point projections then we should be able to estimate the single motion parameters.

## 2.1 Estimation of the Rotation

There are several methods to estimate rotation of a camera from a set of two images. Vanishing points can be used to estimate the rotation matrix [11]. The idea is to use points at infinity that do not experience any image shifts due to translation. In our approach, we use different way to estimate the rotation that converts the imaged points into their normalized direction vectors  $\mathbf{n}_i$  (Fig. 1). This allows us a direct calculation of rotation as described below and additionally provides an easy extension to omnidirectional cameras, where the imaged points can lie on a half-sphere around the focal point of the camera. We describe the algorithm in more detail in the following text.

The camera quantizes the projected information with the resolution of its chip  $(s_x, s_y)$ . We can tell from the Eq. (1) that a motion  $\Delta \vec{T}$  becomes less and less observable for large values of  $z$ . That means that distant points to the camera experience only small shifts in their projected position due to the translational motion of the camera (Fig. 2).

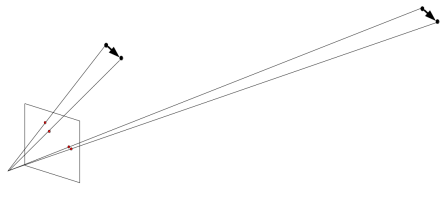


**Fig. 2.** The change in the imaged position for a similar motion in 3D changes with the distance of the observed point to the camera.

The motion becomes not detectable once the resulting image shift falls below the detection accuracy of the camera. Depending on the camera chip resolution  $(s_x, s_y)$  and motion parameters between two frames  $T_m$ , we can define a set of such point  $P_{k\infty}$  in the actual values as points in the distance  $Z_\infty$ :

$$Z_\infty = \frac{f}{s_x} T_m \quad (6)$$

We assumed in (6) that the pixels  $(s_x, s_y)$  are square or the smaller of the both values needs to be taken into account. Additionally, we assumed that the largest observed motion component occurs for motions coplanar to the image plane and that the feature detection works with the accuracy of up to one pixel. We see that for a typical camera setup with a pixel size of  $s_x = 11\mu m$  and a focal length of  $f = 8mm$  objects as close as 14m cannot be detected at motion speeds lower than  $T_m = 2cm/frame$ . This is a typical speed of a mobile robot in the scene. Typically, this value is significantly smaller because the motion component parallel to the image plane for a camera looking forward is smaller (Fig. 3)

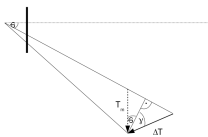


**Fig. 3.** Motion component  $T_m$  that can be observed in the image.

We can calculate the motion value  $T_m$  from the actual motion of the vehicle  $\Delta T$  in Fig. 3 to

$$T_m = \frac{\cos \gamma}{\cos \varphi} \Delta T \quad (7)$$

Therefore, the typical observed motion  $T_m$  is smaller than the value assumed above for a motion observed by a camera looking parallel to the motion vector  $\Delta T$ . This would correspond to a camera looking to the side. An important observation is that  $T_m$  is not only scaled by the distance to the observed point but the angle  $\gamma$  is important for the actual observability of a point motion. We see from this equation directly that a radial motion as it is the case for points along the optical center but also any other motion along the line of projection lets a point render part of the  $\{P_{k\infty}\}$  set of points, from which the translation cannot be calculated.

We use this observation to subdivide the observed points in the camera image into points which are in the distance larger than  $Z_\infty$  in (6) and those that are closer than this value. We use the Kanade-Lucas tracker (KLT) to track image points in a sequence of images acquired by a monocular camera system. The scene depicted in Fig. 4 contains both physical points  $\{P_{lT}\}$  that let observe both motion types translation and rotation, and points  $\{P_{k\infty}\}$  where we observe only the result of the rotation. Before we explain, how we decide which points belong to which set, we make the observation that for the point set  $\{P_{k\infty}\}$  the equation (5) simplifies to

$$\begin{aligned} \forall \{P_{k\infty}\}: \quad \lambda'_i \vec{n}_i &= \lambda_i R^T \vec{n}_i, \quad \text{with} \quad \lambda'_i \simeq \lambda_i \\ &\Rightarrow \quad \vec{n}_i = R^T \vec{n}_i \end{aligned} \quad (8)$$

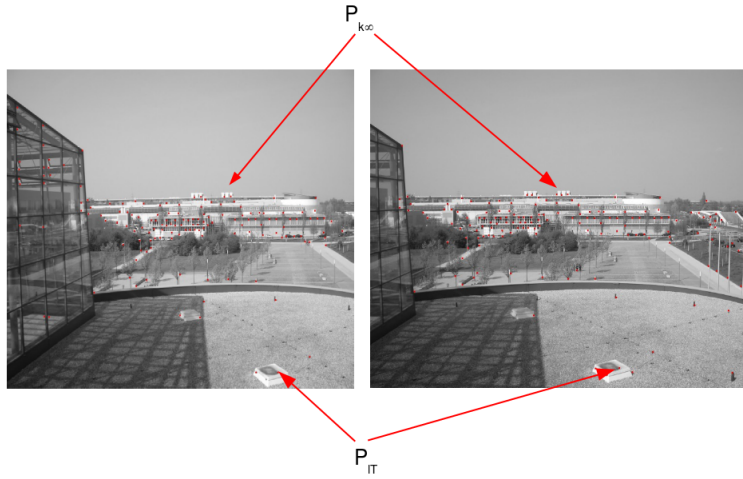


**Fig. 4.** We use Kanade-Lucas tracker (KLT) to track points in a sequence of outdoor images.

It is known that the matrix  $\tilde{\mathbf{R}}$  and the vector  $\mathbf{T}$  between two 3D point sets  $\{P_i\}$  and  $\{P_i^*\}$  can be recovered by solving the following least-square problem for  $N$  landmarks

$$\min_{\tilde{\mathbf{R}}, \mathbf{T}} \sum_{i=1}^N \|\tilde{\mathbf{R}}P_i + \mathbf{T} - P_i^*\|^2, \quad \text{subject to } \tilde{\mathbf{R}}^T \tilde{\mathbf{R}} = I. \quad (9)$$

Such a constrained least squares problem can be solved in closed form using quaternions [5,10], or singular value decomposition (SVD) [4,1,5,10].

The SVD solution proceeds as follows. Let  $\{P_i\}$  and  $\{P_i^*\}$  denote lists of corresponding vectors and define

$$\bar{P} = \frac{1}{n} \sum_{i=1}^n P_i, \quad \bar{P}^* = \frac{1}{n} \sum_{i=1}^n P_i^*, \quad (10)$$

that is,  $\bar{P}$  and  $\bar{P}^*$  are the centroids of  $\{P_i\}$  and  $\{P_i^*\}$ , respectively. Define

$$P'_i = P_i - \bar{P}, \quad P'^*_i = P_i^* - \bar{P}^*, \quad (11)$$

and

$$\tilde{\mathbf{M}} = \sum_{i=1}^n P'^*_i P'^*_i{}^T. \quad (12)$$

In other words,  $\frac{1}{n} \tilde{\mathbf{M}}$  is the sample cross-covariance matrix between  $\{P_i\}$  and  $\{P_i^*\}$ . It can be shown that, if  $\tilde{\mathbf{R}}^*$ ,  $\mathbf{T}^*$  minimize (9), then they satisfy

$$\tilde{\mathbf{R}}^* = \operatorname{argmax}_{\tilde{\mathbf{R}}} \operatorname{tr}(\tilde{\mathbf{R}}^T \tilde{\mathbf{M}}) \quad (13)$$

Since we subtract the mean value  $\bar{P}$  in (11), we remove any translation component leaving just a pure rotation.

Let  $(\tilde{U}, \tilde{\Sigma}, \tilde{V})$  be a SVD of  $\tilde{M}$ . Then the solution to (9) is

$$\tilde{\mathbf{R}}^* = \tilde{\mathbf{V}}\tilde{\mathbf{U}}^T \quad (14)$$

We use the solution in equation (14) as a least-square estimate for the rotation matrix  $\mathbf{R}$  in (8). The 3D direction vectors  $\{n_i\}$  and  $\{n'_i\}$  are used as the point sets  $\{P_i\}$  and  $\{P_i^*\}$  in the approach described above. It is important to use the  $\vec{n}_i$  vectors and not the  $\vec{k}_i$  vectors from (3) here.

The reader may ask, how can we make this distinction which points belong to  $\{P_{k\infty}\}$  not knowing the real radial distances  $\lambda_i$  to the imaged points like the ones depicted in Fig. 4? It is possible to use assumptions about the field of view of the camera to answer this question, where points at the horizon appear in well defined parts of the image. We apply a generic solution to this problem involving the Random Sample Consensus (RANSAC). It was introduced by Bolles and Fischler [2]. RANSAC picks a minimal subset of 3 tracked points and calculates the least-square approximation of the rotation matrix for them (14). It enlarges the set with consistent data stepwise. We used following Lemma to pick consistent points for the calculation of  $\mathbf{R}$ .

*Lemma:* All points used for the calculation of  $\mathbf{R}$  belong to the set  $\{P_{k\infty}\}$ , iff the calculated  $\mathbf{R}$  warps the appearance of the point features  $\{n_i\}$  to the appearance in the second image  $\{n'_i\}$ .

The resulting image error for correct points goes to zero after applying the 3D rotation matrix to their corresponding direction vectors. Note that we estimate here directly the 3 rotational parameters of the camera system and not the rotation in the image space like most other approaches.

We can validate it at the following example in Fig. 5. We generated a set of feature points in a close range to the camera in a distance 1-4m in front of the camera. These points are marked with (+) in the images. A second set of points was placed in a distance 25-35m in front of the camera and these points are marked with (x). We estimated the rotational matrix from a set of direction vectors  $n_i$  estimated with RANSAC that matched the (x) points. These points represent the  $\{P_{k\infty}\}$  set of our calculation. The calculated 3D rotation matrix had a remaining error of  $(-0.1215^\circ, 0.2727^\circ, -0.0496^\circ)$ .

We used the rotation matrix to compensate all direction vectors in the second image  $\{n'_i\}$  for the influence of rotation during the camera motion. Fig. 6 depicts the positions of all features after compensation of the rotation influence. We see that as we already expected above the distant features were moved to their original positions. These features do not give us any information about the translation. They should not be used in the following processing. The close features (marked with '+') in Fig. 6 still have a residual displacement in the image after the compensation of the rotation that gives us information about the translation between the two images.

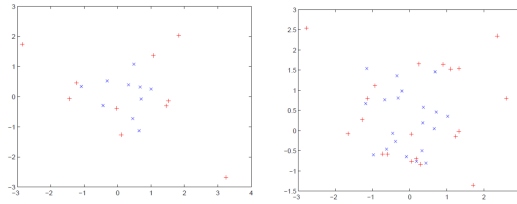


**Fig. 5.** Two synthetic sets of feature positions with close (+) and distant points (x) with a camera translation by  $\Delta T = (0.3, 0.2, 0.4)^T$  [m] and a rotation around the axes by  $(10^\circ, 2^\circ, 5^\circ)$ .

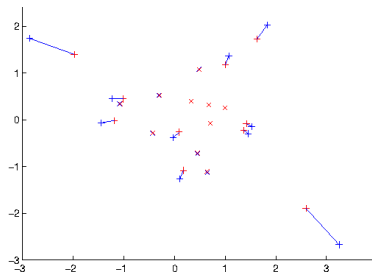


**Fig. 6.** Features from Fig. 5 compensated for rotation estimated from (x) feature positions.

## 2.2 Estimation of the Translation

In the equation (5), we identified two possible motion components in the images. It is known that the 3D rotation of the camera relative to the world can always be calculated, but the distances to the imaged points can only be calculated once a significant motion between the frames is present (see Fig. 6). We need some remaining points with significant displacement between the images (after they were compensated for rotation) to estimate the translation parameters. We estimate the translation of the camera from the position of the epipoles.

We know from Fig. 1 that the camera measures only the direction  $n_i$  to the imaged point but loses the radial distance  $\lambda_i$ . Therefore, we know only the direction to both points  $(P_1, P_2)$  for the left camera position in Fig. 7. If we find correspondences in both cameras then we know that the corresponding point lies somewhere on a line starting at the projection of the focal point of the right camera in the left image (epipole) and that it intersects the image plane of the right camera in the corresponding point. The projection of this line in the left image is called the epipolar line. We know that both corresponding points lie on the epipolar line and that the epipole defines the beginning of the line segment. Therefore, it is possible to find the position of the epipole by intersecting two such lines since all epipolar lines share the same epipole. Since the points  $(P_i, F_1, F_2)$



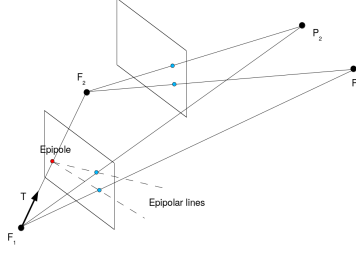


**Fig. 7.** In case that the camera is moved by a pure translation, the direction of the epipole  $T$  defines the direction of the translational motion.

define a plane, all possible projections of the given point while travelling along the line  $\overline{F_1F_2}$  will appear on the epipolar line.

We need at least two corresponding point pairs in the  $\{P_{lT}\}$  to estimate the position of the epipole in the image. For each of the line pairs, we calculate the following equation using the 2D projections  $\overrightarrow{k_{ip}}$  of the  $\overrightarrow{k_i}$  vectors from the equation (3) on the image plane. As simplification, we write in the following equation (15)  $\overrightarrow{k_i}$  for them, but we mean the 2D projections.

$$\begin{aligned} \overrightarrow{k_a} + \mu * (\overrightarrow{k'_a} - \overrightarrow{k_a}) &= \overrightarrow{k_b} + \nu * (\overrightarrow{k'_b} - \overrightarrow{k_b}) \\ \begin{pmatrix} \mu \\ \nu \end{pmatrix} &= \begin{pmatrix} \overrightarrow{k_a} - \overrightarrow{k'_a} & \overrightarrow{k_b} - \overrightarrow{k'_b} \end{pmatrix}^{-1} \cdot (\overrightarrow{k_a} - \overrightarrow{k_b}) \end{aligned} \quad (15)$$

We can estimate the image position of the epipole  $E_p$  from the estimated values  $(\mu, \nu)$  using the 3D versions of the vectors  $\overrightarrow{k_i}$  to for example:

$$\overrightarrow{E_p} = \overrightarrow{k_a} + \mu * (\overrightarrow{k'_a} - \overrightarrow{k_a}) \quad (16)$$

Note that the position of the epipole is identical for both images after the compensation of rotation. The epipole defines the direction of motion between the two cameras as depicted in Fig. 7. It is a known fact that we can reconstruct the motion parameters only up to an unknown scale from a monocular camera. Therefore, all we can rely on is the direction of motion

$$\overrightarrow{T} = \frac{c}{\|\overrightarrow{E_p}\|} \overrightarrow{E_p} \quad (17)$$

The value  $c$  in (17) can have a value of  $\pm 1$  depending on the direction in which the corresponding points move in the images. If the corresponding point moves away from the epipole then we assume  $c=1$  and if the corresponding point moves toward the epipole then we assume  $c=-1$ . This explains, why we get two identical epipoles for both translated images. These images have similar translation vectors. The only difference is the sign ( $c$ -value).

For the example from Fig. 6, we calculate the position of the epipole to be  $\overrightarrow{E_p} = (0.7, 0.36, 1)^T$  that matches exactly the direction of the motion that we

used to create the data. We can get multiple solutions for the position of the epipole in the image. The different results originate from intersection of different line lengths, which allows to pick the lines with the longest image extension to reduce the detection error and increase the accuracy. A better option is to use a weighted  $\omega_i$  average of the estimated values  $E_{p_i}$ . The weight  $\omega_i$  depends on the minimal length  $l_i$  of the both line segments and it is calculated to:

$$\omega_i = \begin{cases} \frac{l_i}{L}, & l_i < L \\ 1, & l_i \geq L \end{cases} \Rightarrow \vec{E}_p = \frac{\sum_i (\omega_i \vec{E}_{p_i})}{\sum_i \omega_i} \quad (18)$$

The value L is chosen depending on the actual accuracy of the feature detection. We set it to L=12 pixels in our system, which means that displacements larger than 12 pixels for translation will be considered accurate.

### 2.3 Calculation of the Translational Error

We need to estimate the covariance of the resulting pose estimation directly from the quality of the data in the images. It is obvious that accuracy increases with the increasing length of the image vectors of the optical flow. In these cases, detection errors have smaller influence. In general, the vectors of the translational field do not intersect in one point (the epipole) as in the ideal case, but they intersect in an area around the epipole. The area gets smaller if the angle between the vectors is close to  $90^\circ$  and increases the more the vectors become parallel to each other. Parallel vectors intersect in infinity and does not allow any robust motion estimation in our system.

We can estimate the variance of the resulting translational vector from the variance of the intersecting point vector pairs of the translational vector field. It is very important to provide this value as an output of the system, because calculated translational value may be ill-conditioned due to very short almost parallel vectors that may intersect in a large area around the actual epipole position.

## 3 Results

We applied the presented system on a variety of images in indoor and outdoor scenarios. The system was able to calculate both the rotation matrix R in all cases and the direction of the translation depending on the matching criterions in the RANSAC process calculating the inliers (points used for rotation) and outliers based on compensation of the rotation and evaluation of the resulting re-projection error. This matching can allow deviations of the position of the reprojected points. In case of poor camera calibration and/or poor feature detection the matching must be set to higher values allowing larger variations. This requires automatically a larger translations between the frames.

We validated the system on synthetic and real images to estimate the accuracy of the system.

### 3.1 Simulation Results

We tried to estimate the accuracy of the algorithm assuming a sub-pixel accuracy in point detection in the images. We added white noise to the ideal values with  $\sigma^2 = 0.05$ . We added 20 outliers to the matches provided to the algorithm. We validated it on 2000 images. We observed following accuracies:

average number of matches	89.7725
average rotation error around the x-axis	0.0113°
average rotation error around the y-axis	0.0107°
average rotation error around the z-axis	0.0231°
number of failed estimates of rotation	0 from 2000
number of failed estimates of translation	0 from 2000
average error in the direction of the estimated translation vector	2.5888°

The system provides robust estimates of the pose even under presence of outliers, which is an important extension to the typical structure from motion algorithm.

### 3.2 Tests on Real Images

We tested the system using a calibrated digital camera that we used to acquire a sequence of images in different scenarios. We ran a C++-implementation of the KLT-tracker on this sequence of images that created a list of tracked positions for single image features. We used this lists in Matlab to evaluate the rotation and translation parameters.

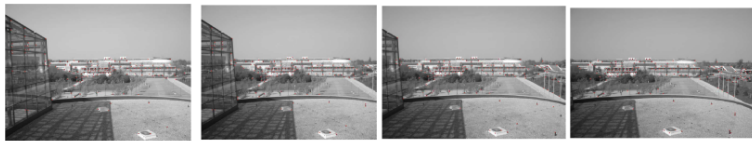


**Fig. 8.** Horizontal sweep of the camera with mostly rotation.

For the sequence in Fig. 8, we obtained the following results:

rotation $(\alpha, \beta, \gamma)$ in [°]	inlier	outlier	error
(2.132,-0.077,0.108)	49	5	0.003066
(4.521,-0.007,0.0751)	11	7	0.003874
(1.9466,0.288,-0.071)	56	6	0.004



**Fig. 9.** Rotation around several axes simultaneously.

We tested the estimation of significant rotation around all axes in Fig. 9 with the following results:

rotation $(\alpha, \beta, \gamma)$ in $[\circ]$	inlier	outlier	error
(1.736,-2.3955,6.05)	24	1	0.0024
(1.08,0.64,4.257)	87	0	0.0012
(2.2201,-0.2934,6.7948)	56	6	0.004

The second sequence in Fig. 9 shows the ability of the system to capture the rotation of the camera correctly in all three possible rotational degrees of freedom in each frame without any iterations necessary. Due to the page limit, we cannot show our further results in indoor scenarios, where we were able to provide some significant translation that allows a simultaneous estimation of the translation direction.

We tested the system on real images taken from a car driven on our campus and through the city of Garching close to Munich.

Fig. 10 depicts the results of real navigation in a city and campus scenario. The red points in the top left images are the points used to estimate the rotation parameters while the green points are the points used to estimate the translation. The top right image shows the resulting translational optical flow and the position of the estimated epipole as a black circle with a cross. The estimated motion parameters with accuracies are also shown in Fig. 10.

## 4 Conclusions and Future Work

We presented a way to calculate pose and covariance values for camera-based navigation with a monocular camera. The approach calculates directly the 6DoF motion parameters from a pair of images and estimates the accuracy for the estimated values that allows a correct fusion of the resulting values in higher level fusion algorithms used for SLAM, like Kalman Filters. We provide the mathematical framework that allows to subdivide tracked feature points into two sets of points that are close to the sensor and whose position change in the image due to a combined rotation and translation motion, and points that are far away and experience only changes due to the rotation of the camera. The presented system was tested on synthetic and real world images proving the validity of this concept.

The system is able to calculate the 6DoF parameters in every camera step without any necessity for initialization of scene structure or initial filtering of uncertainties. In the next step, we will test the translation estimates using external references for motion of the real camera system and integrate the sensor into our VSLAM system.

## References

1. K. S. Arun, T. S. Huang, and S. D. Blostein, Least-squares fitting of two 3-D point sets, *IEEE Trans. Pat. Anal. Machine Intell.*, vol. 9, pp. 698–700, 1987.
2. Martin Fischler, Robert Bolles, Random Sample Consensus: A Paradigm for Model Fitting with Applications to Image Analysis and Automated Cartography. *Commun. ACM*, 24(6), pp. 381–395, 1981.
3. Andrew J. Davison. Real-Time Simultaneous Localisation and Mapping with a Single Camera. *Proc Internation Conference on Computer Vision*, Volume 2, pages 1403–1412, 2003.
4. B. K. P. Horn, H. M. Hilden, and S. Negahdaripour, “Closed-form solution of absolute orientation using orthonormal matrices,” *J. Opt. Soc. Amer.*, vol. A-5, pp. 1127–1135, 198.
5. B. K. P. Horn, “Closed-form solution of absolute orientation using unit quaternion,” *J. Opt. Soc. Amer.*, vol. A-4, pp. 629–642, 1987.
6. B. K. P. Horn. *Robot Vision*. MIT Press, 1986.
7. H. C. Longuet-Higgins. *A computer algorithm for reconstructing a scene from two projections*. *Nature*, vol. 293, no. 10, pp. 133135, Sept. 1981.
8. David Nister. A Minimal Solution to the Generalised 3-Point Pose Problem. *CVPR 2004*, 2004.
9. S. Thrun. Learning metric-topological maps for indoor mobile robot navigation. *Artificial Intelligence*, 99(1):21–71, 1998.
10. M. W. Walker, L. Shao, and R. A. Volz, “Estimating 3-D location parameters using dual number quaternions,” *CVGIP: Image Understanding*, vol. 54, no. 3, pp. 358–367, 1991.
11. R. Hartley and A. Zisserman. *Multiple View Geometry in Computer Vision*. Cambridge University Press, Second Edition.

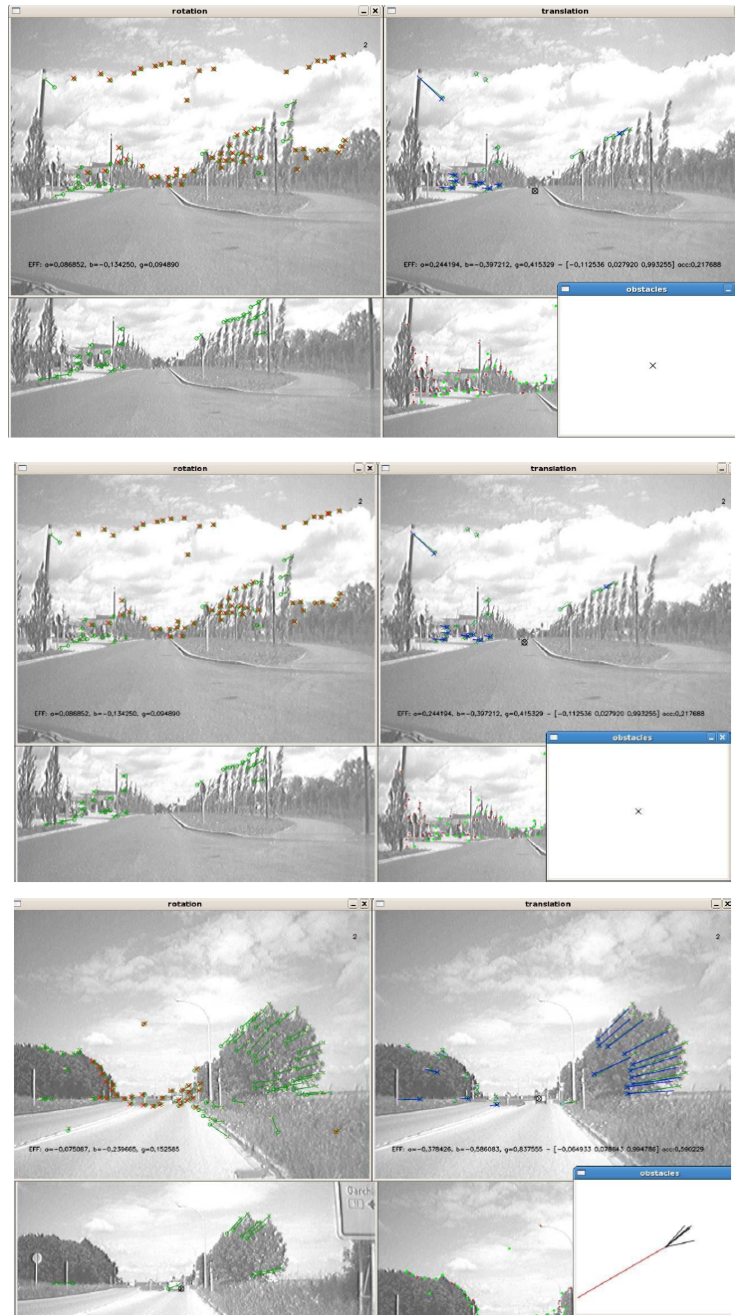


**Fig. 10.** Shown are two screen-shots of our working navigation system showing the results for two scene examples (top) drive through the Garching campus, (bottom) drive through the city of Garching.